

RESEARCH ARTICLE

# Neutralization of *Clostridium difficile* toxin B with V<sub>H</sub>H-Fc fusions targeting the delivery and CROPs domains

Greg Hussack<sup>1\*</sup>, Shannon Ryan<sup>1</sup>, Henk van Faassen<sup>1</sup>, Martin Rossotti<sup>1</sup>, C. Roger MacKenzie<sup>1</sup>, Jamshid Tanha<sup>1,2,3</sup>

**1** Human Health Therapeutics Research Centre, National Research Council Canada, Ottawa, Ontario, Canada, **2** Department of Biochemistry, Microbiology and Immunology, University of Ottawa, Ottawa, Ontario, Canada, **3** School of Environmental Sciences, University of Guelph, Guelph, Ontario, Canada

\* [Greg.Hussack@nrc-cnrc.gc.ca](mailto:Greg.Hussack@nrc-cnrc.gc.ca)



## Abstract

An increasing number of antibody-based therapies are being considered for controlling bacterial infections, including *Clostridium difficile* by targeting toxins A and B. In an effort to develop novel *C. difficile* immunotherapeutics, we previously isolated several single-domain antibodies (V<sub>H</sub>Hs) capable of toxin A neutralization through recognition of the extreme C-terminal combined repetitive oligopeptides (CROPs) domain, but failed at identifying neutralizing V<sub>H</sub>Hs that bound a similar region on toxin B. Here we report the isolation of a panel of 29 V<sub>H</sub>Hs targeting at least seven unique epitopes on a toxin B immunogen composed of a portion of the central delivery domain and the entire CROPs domain. Despite monovalent affinities as high as  $K_D = 70$  pM, none of the V<sub>H</sub>Hs tested were capable of toxin B neutralization; however, modest toxin B inhibition was observed with V<sub>H</sub>H-V<sub>H</sub>H dimers and to a much greater extent with V<sub>H</sub>H-Fc fusions, reaching the neutralizing potency of the recently approved anti-toxin B monoclonal antibody bezlotoxumab in *in vitro* assays. Epitope binning revealed that several V<sub>H</sub>H-Fcs bound toxin B at sites distinct from the region recognized by bezlotoxumab, while other V<sub>H</sub>H-Fcs partially competed with bezlotoxumab for toxin binding. Therefore, the V<sub>H</sub>Hs described here are effective at toxin B neutralization when formatted as bivalent V<sub>H</sub>H-Fc fusions by targeting toxin B at regions both similar and distinct from the bezlotoxumab binding site.

## OPEN ACCESS

**Citation:** Hussack G, Ryan S, van Faassen H, Rossotti M, MacKenzie CR, Tanha J (2018) Neutralization of *Clostridium difficile* toxin B with V<sub>H</sub>H-Fc fusions targeting the delivery and CROPs domains. PLoS ONE 13(12): e0208978. <https://doi.org/10.1371/journal.pone.0208978>

**Editor:** Yung-Fu Chang, Cornell University, UNITED STATES

**Received:** September 23, 2018

**Accepted:** November 28, 2018

**Published:** December 12, 2018

**Copyright:** © 2018 Hussack et al. This is an open access article distributed under the terms of the [Creative Commons Attribution License](https://creativecommons.org/licenses/by/4.0/), which permits unrestricted use, distribution, and reproduction in any medium, provided the original author and source are credited.

**Data Availability Statement:** All relevant data are within the manuscript and its Supporting Information files.

**Funding:** This study was funded by the National Research Council Canada. The funder had no role in study design, data collection and analysis, decision to publish, or preparation of the manuscript.

**Competing interests:** The authors have declared that no competing interests exist.

## Introduction

*Clostridium difficile* is a Gram-positive spore-forming bacterium that continues to be a problematic nosocomial pathogen. The symptoms of gastrointestinal *C. difficile* infections can range from mild diarrhea to pseudomembrane colitis and death. The spore-forming nature of the pathogen coupled with an ability to rapidly colonize patients on broad-spectrum antibiotics presents a significant challenge to infection control in healthcare settings. Healthcare associated costs of managing *C. difficile* infection were estimated to exceed a staggering \$4.5 billion annually in the US alone [1]. Despite the introduction of therapies that include new antibiotic modalities, fecal transplantation and antibody-based immunotherapy, efficacy limitations remain which necessitate the continuous search for more potent therapeutic agents [2,3,4].

*C. difficile* secretes two large toxins (TcdA and TcdB) that act upon the epithelial cells lining the gastrointestinal tract by first internalizing and then inactivating Rho/Ras proteins, which leads to cell-cytoskeleton disruption and ultimately a loss of epithelial barrier function, severe inflammation and apoptosis [5,6]. TcdA and TcdB are each four-domain proteins composed of an N-terminal glucosyltransferase domain, a central autoprotease cutting domain, a neighboring central delivery/translocation domain and a C-terminal region referred to as the combined repetitive oligopeptides (CROPs) domain. These two toxins, along with transferase toxin (CDT), are considered the primary virulence factors of *C. difficile* and have been targeted by toxin-binding polymers, vaccines and antibodies as strategies to control *C. difficile*-associated disease [5]. With respect to antibodies a number of anti-toxin formats have been explored, including intravenous immunoglobulin therapy, IgG, IgA, IgY, single-chain fragment variable (scFv) and single-domain antibodies (sdAbs) [2,7]. Recently, the anti-TcdB monoclonal antibody (mAb) bezlotoxumab was FDA-approved for the treatment of recurrent *C. difficile* infection [8,9].

In an effort to develop novel antibody-based therapeutics for *C. difficile* infection, our group and others have explored the use of sdAbs as potent anti-toxin neutralizing agents [10,11,12,13,14,15,16,17,18,19]. Camelid-sourced sdAbs (V<sub>H</sub>Hs or Nanobodies) are recombinant antibody fragments that offer the benefits of full-sized mAbs—high target affinity and specificity—with unique properties, most notably their amenability to tandem formatting in various geometries such that multi-specificities can be attained within a single molecule [20,21,22]. We previously isolated several moderate-affinity llama V<sub>H</sub>Hs that targeted the C-terminal CROPs domain (also referred to as the receptor binding domain or RBD) of TcdA (aa 2304–2710) that were neutralizers of TcdA as single V<sub>H</sub>Hs or in combination [10]. At the same time, immunization with a small C-terminal fragment of the TcdB CROPs domain (aa 2286–2366) failed to produce neutralizing V<sub>H</sub>Hs.

Here, we immunized a llama with a recombinant TcdB fragment (aa 1751–2366) that encompasses a portion of the central delivery/translocation domain (aa 1751–1833) and the entire CROPs domain (aa 1834–2366). We hypothesized that extending our previous immunogen design to include a portion of the delivery/translocation domain and the full-length CROPs domain may lead to neutralizing antibodies. This is supported by recent reports showing TcdB binding the frizzled (FZD2) family of Wnt receptors [23,24] and the poliovirus receptor-like 3 (PVRL3) receptor [25] through the central delivery/translocation domain, and TcdB binding the chondroitin sulfate proteoglycan 4 (CSPG4) receptor [26] through a region adjacent to the CROPs domain. In addition, several earlier studies showed the isolation of neutralizing antibodies to the CROPs region of TcdB [15,27,28]. Despite isolating numerous V<sub>H</sub>Hs with affinities as high as  $K_D = 70$  pM, none of the monomeric antibodies were capable of preventing TcdB-induced cytotoxicity in cell-based assays. However, when reformatted as Fc-fusions, several V<sub>H</sub>H-Fcs were transformed into potent TcdB neutralizers on par with the neutralizing efficacy of the recently approved anti-TcdB mAb bezlotoxumab. Thus, TcdB-binding V<sub>H</sub>Hs targeting a fragment of the delivery domain and the complete CROPs domain are effective neutralizers when presented in the context of larger bivalent V<sub>H</sub>H-Fc fusions, presumably due to steric and/or avidity effects not afforded to monomeric V<sub>H</sub>Hs.

## Materials and methods

### Llama immunization, serum fractionation and serology

Recombinant TcdB (aa 1751–2366; hereafter referred to as TcdB<sub>1751-2366</sub>) was a generous gift from Dr. Kenneth Ng (University of Calgary, Calgary, AB, Canada). A llama was immunized with 100 µg of TcdB<sub>1751-2366</sub> per injection, following a similar immunization schedule and

adjuvanted as previously reported [29]. Serum from blood drawn 42 days post immunization was tested for binding to TcdB<sub>1751-2366</sub> by ELISA essentially as described [10]. Serum was fractionated according to established protocols with protein G and protein A affinity columns [30] and conventional and heavy-chain IgG fractions tested for TcdB<sub>1751-2366</sub> binding by ELISA [10]. The ability of polyclonal fractions to neutralize TcdB VPI 10463 (List Biological Laboratories) was examined by Vero cell toxin inhibition assays, essentially as described for TcdA [19] with minor modifications. Vero cell monolayers were incubated with a final TcdB concentration of 10 pM (2.7 ng/mL) or 30 pM (8.1 pg/mL) and 1 μM of day 42 fractionated serum for 72 h at 37°C and 5% CO<sub>2</sub> before addition of WST-1 cytotoxicity reagent (Roche, Mississauga, ON, Canada) for 30 min and subsequent absorbance measurement at 450 nm.

### Research involving animals

All procedures involving llamas and their care were approved by the National Research Council Canada Animal Care Committee and by the Animal Care Committee of Cedarlane Laboratories who is licensed by the Ontario Ministry of Agriculture, Food and Rural Affairs.

### Library construction, V<sub>H</sub>H isolation and expression

Lymphocytes obtained from serum drawn 42 days post immunization served as a starting point for phagemid library construction. RNA extraction, cDNA synthesis, two rounds of PCR, restriction digestion, ligation into the pMED1 phagemid vector, transformation of electrocompetent *E. coli* and preparation of library phage were all performed as described [10,30]. V<sub>H</sub>Hs were then selected by two approaches. In the first approach, TcdB<sub>1751-2366</sub> was coated directly onto microtiter plate wells, plates were blocked with 5% non-fat skimmed milk in PBS-T (PBS + 0.5% (v/v) Tween 20), and library phage applied, washed and eluted with 0.1 M triethylamine, all essentially as reported [10], for three rounds. In the second approach, TcdB<sub>1751-2366</sub> was first biotinylated (TcdB<sub>1751-2366</sub>-Biotin) using a commercial EZ-Link<sup>TM</sup> Sulfo-NHS-Biotinylation Kit (ThermoFisher, Ottawa, ON, Canada), according to the manufacturer's instructions, and confirmed by Western blotting by probing with streptavidin (SA) conjugated with AP (ThermoFisher). Next, library phage were incubated with TcdB<sub>1751-2366</sub>-Biotin (5 nM) in a 1.5 mL Eppendorf tube for 10 min before addition of non-biotinylated TcdB<sub>1751-2366</sub> competitor (2.5 μM) for 10 min. The mixture was then applied to streptavidin coated microtiter plates (ThermoFisher) for 5 min before a series of washes with PBS and PBS-T and elution with 0.1 M triethylamine. In each subsequent round the concentration of TcdB<sub>1751-2366</sub>-Biotin target was reduced and the incubation time with TcdB<sub>1751-2366</sub> competitor increased, except for the fourth round in which the incubation time was held at 60 min. Eluted phage clones displaying V<sub>H</sub>Hs from both isolation methods were tested for binding to immobilized TcdB<sub>1751-2366</sub> in monoclonal phage ELISA as described [10] and those clones producing the highest absorbance (450 nm) were sequenced, subcloned into the pSJF2H expression vector [10], and expressed and purified from *E. coli* by IMAC [10,30]. Purified V<sub>H</sub>Hs were probed by Western blotting using an α-His tag specific IgG conjugated with AP (ThermoFisher).

### V<sub>H</sub>H characterization

The aggregation state of V<sub>H</sub>Hs was assessed by size-exclusion chromatography (SEC) using a Superdex<sup>TM</sup> 75 Increase column (GE Healthcare, Mississauga, ON, Canada) as described [10,31]. V<sub>H</sub>H thermal unfolding and refolding were examined by circular dichroism spectroscopy, essentially as reported [31], with the exception of data collection every 0.2°C and the V<sub>H</sub>Hs were allowed to cool at 25°C for 3 h before the second thermal melt was performed. The monovalent binding affinities of V<sub>H</sub>Hs were determined using a Biacore 3000 surface plasmon

resonance (SPR) instrument (GE Healthcare) and the Biotin CAPture Kit (GE Healthcare). Approximately 900 resonance units (RUs) of TcdB<sub>1751-2366</sub>-Biotin were captured before flowing a two-fold dilution series of SEC-purified V<sub>H</sub>Hs (concentrations ranging from as low as 0.13–2 nM to as high as 31.3–500 nM) over the TcdB<sub>1751-2366</sub>-Biotin surface using single-cycle kinetic analysis. All experiments were performed in HBS-EP buffer (10 mM HEPES, pH 7.4, 150 mM NaCl, 3 mM EDTA, 0.005% (v/v) Surfactant P20; GE Healthcare) at 25°C at a flow rate of 30 µL/min, with a contact time of 2 min and dissociation time of 10 min. Surfaces were regenerated according to the Biotin CAPture Kit instructions (Regeneration stock 1 and 2, at 10 µL/min). Reference flow cell subtracted sensorgrams were fit to a 1:1 binding model using the BIAevaluation 4.1 software (GE Healthcare). V<sub>H</sub>H epitope binning was also performed by SPR on TcdB<sub>1751-2366</sub>-Biotin captured surfaces by injection of the first V<sub>H</sub>H at 10×  $K_D$  concentration for 2 min followed immediately by injection of a mixture of the first V<sub>H</sub>H + a second V<sub>H</sub>H at 10×  $K_D$  concentration for 2 min, all at a flow rate of 30 µL/min. Binning experiments were also performed in the reverse format (i.e., V<sub>H</sub>H2 followed by V<sub>H</sub>H2 + V<sub>H</sub>H1). The ability of V<sub>H</sub>Hs to neutralize TcdB VPI 10463 was examined by Vero cell toxin inhibition assays, essentially as described above for fractionated serum. Vero cell monolayers were incubated with a final TcdB concentration of 1 pM (270 pg/mL) and 1 µM of V<sub>H</sub>H for 72 h at 37°C and 5% CO<sub>2</sub> before addition of WST-1 cytotoxicity reagent (Roche) for 30 min and subsequent absorbance measurement at 450 nm. Before performing TcdB inhibition assays that involved V<sub>H</sub>Hs, dimers and Fc-fusions, dose-response experiments were always conducted to identify a working TcdB concentration that provided ~90% toxicity to account for batch-to-batch variability in TcdB potency.

### Generation and characterization of V<sub>H</sub>H-V<sub>H</sub>H dimers

Using the three highest affinity V<sub>H</sub>Hs targeting unique epitopes (B39, B74 and B167) all V<sub>H</sub>H-V<sub>H</sub>H dimer formats were constructed by splice overlap extension PCR, essentially as described [31], before ligation into pSJF2H expression vector. Each dimer was separated by a 25 amino acid linker (Gly<sub>4</sub>Ser)<sub>5</sub> and contained a C-terminal His<sub>6</sub> tag for purification. Dimers were expressed in 1 L *E. coli* cultures, extracted from the periplasm by osmotic shock, purified by IMAC and assessed for purity and aggregation by SDS-PAGE, Western blot and SEC with a Superdex 200 Increase column (GE Healthcare), according to standard methods. When V<sub>H</sub>H-V<sub>H</sub>Hs showed higher order aggregates or signs of degradation by SEC, the non-aggregating monomer peaks were collected and used for subsequent assays. The thermal unfolding temperature of each dimer was determined as described above for monomer V<sub>H</sub>Hs. The dissociation rate of each V<sub>H</sub>H-V<sub>H</sub>H dimer was determined by SPR using conditions described above for binding to TcdB<sub>1751-2366</sub>-Biotin captured surfaces. Briefly, dimers and control monomers were injected at 1 nM for 5 min before 30 min of dissociation, all at 25°C with a flow rate of 30 µL/min and in HBS-EP buffer (GE Healthcare). Dissociation phases were fit to a 1:1 dissociation model using the BIAevaluation 4.1 software (GE Healthcare) in order to calculate  $k_{d,s}$  (s<sup>-1</sup>). The ability of V<sub>H</sub>H-V<sub>H</sub>H dimers to neutralize TcdB (List Biological Laboratories) was examined by Vero cell toxin inhibition assays as described above for fractionated serum and V<sub>H</sub>H monomers. A final TcdB concentration of 3 pM (810 pg/mL), based on dose-response experiments, and a dimer concentration of 1 µM were used. All other assay conditions remained the same. An irrelevant dimer T5/TC9 [32] was used at 1 µM as a negative control while the TcdB-binding mAb bezlotoxumab (MDX-1388) was used at 250 nM as a positive control.

### Generation and characterization of V<sub>H</sub>H-Fc fusions

V<sub>H</sub>Hs fused to the N-termini of human IgG1 Fcs were synthesized and subcloned into the pTT5 vector and expressed through transient transfection of mammalian HEK293-6E cells

before protein A purification, as described [33,34]. Each V<sub>H</sub>H was separated from the IgG1 Fc region by either the human IgG1 hinge or a 35-residue camel/llama  $\gamma$ 2a hinge [35]. The aggregation profiles of V<sub>H</sub>H-Fcs were assessed by SEC using a Superdex 200 column (GE Healthcare). SPR was used to determine the dissociation rates of V<sub>H</sub>H-Fcs by flowing 1 nM of SEC-purified antibody over TcdB<sub>1751-2366</sub>-Biotin surfaces for 2 min, followed by a dissociation time of 30 min, all at 25°C with a 30  $\mu$ L/min flow rate in HBS-EP buffer (GE Healthcare). SPR-based binning experiments between V<sub>H</sub>H-Fcs and MDX-1388 [36] were performed essentially as described above for V<sub>H</sub>H monomers. The ability of V<sub>H</sub>H-Fcs to neutralize TcdB (List Biological Laboratories) was examined by Vero cell toxin inhibition assays as described above for V<sub>H</sub>H monomers and dimers. A final TcdB concentration of 500 fM (135 pg/mL), based on dose-response experiments, and a V<sub>H</sub>H-Fc fusion concentration of 250 nM were used. All other assay conditions remained the same. When two V<sub>H</sub>H-Fc fusions were used in combination for TcdB inhibition, 125 nM of each V<sub>H</sub>H-Fc was added. TcdB and V<sub>H</sub>H-Fcs were not pre-incubated before the addition to Vero cells.

## Results

### Llama immunization, serum fractionation and serology

In an attempt to generate TcdB neutralizing V<sub>H</sub>Hs, we started by immunizing a llama with recombinant TcdB<sub>1751-2366</sub> which consists of a portion of the central delivery/translocation domain and entire CROPs domain (Fig 1A and 1B). Serum drawn 35 days and 42 days post immunization showed a clear response to TcdB<sub>1751-2366</sub> by ELISA (Fig 1C). Serum drawn on day 42 was separated by fractionation into conventional IgG (cIgG; G2 fraction) and heavy-chain IgG (hcIgG; G1 fraction—a long hinge isotype based on SDS-PAGE, and A1 and A2 fractions—a short hinge isotype(s) based on SDS-PAGE, Fig 1D) and showed a typical reactivity pattern by TcdB<sub>1751-2366</sub> binding in ELISA (Fig 1E). The G2 fraction (cIgG) showed the strongest reactivity towards TcdB<sub>1751-2366</sub> with an EC<sub>50</sub> ~ 0.1  $\mu$ g/mL compared to the G1 fraction (hcIgG) with an EC<sub>50</sub> ~ 2  $\mu$ g/mL. A1 and A2 fractions (hcIgG) possessed considerably lower TcdB binding titers. We next examined if the fractionated polyclonal sera could neutralize TcdB in Vero cell cytotoxicity assays. TcdB (10 or 30 pM, final) was added to Vero cells alone or in combination with fractionated serum (1  $\mu$ M, final) for 72 h before addition of WST-1 reagent (Fig 1F). At 30 pM of TcdB the G2 fraction fully inhibited TcdB, while approximately 30% was inhibited by the A2 fraction, 10% by the G1 fraction and no inhibition with A1. A similar pattern was seen when 3-fold less TcdB was used: near complete inhibition with G2 and A2, approximately 30% by G1 and less than 10% by A1. The inhibition pattern largely matches the TcdB binding data (Fig 1E), although the A2 heavy-chain fraction showed greater inhibition than G1, presumably due to the presence of minor IgM contaminants (Fig 1D) that would efficiently neutralize TcdB due to size and valency. We next proceeded with phage display library construction and created a phage display library with a size of ~ 3 x 10<sup>7</sup> independent transformants.

### V<sub>H</sub>H isolation and expression

For the isolation of V<sub>H</sub>Hs, two different selection strategies were used: solution panning (off-rate based selection) and solid-phase panning (Fig 1G). In off-rate based selections 5 nM of biotinylated TcdB<sub>1751-2366</sub> (Fig 1A) was incubated with the phage-displayed V<sub>H</sub>H library followed by addition of a 500-fold molar excess of non-biotinylated TcdB<sub>1751-2366</sub> (2.5  $\mu$ M) for 10 min before capture on streptavidin coated wells, washing and elution in round 1 (Fig 1G). In each subsequent round the amount of biotinylated TcdB<sub>1751-2366</sub> was decreased and the incubation time with non-biotinylated TcdB<sub>1751-2366</sub> competitor increased. For solid-phase

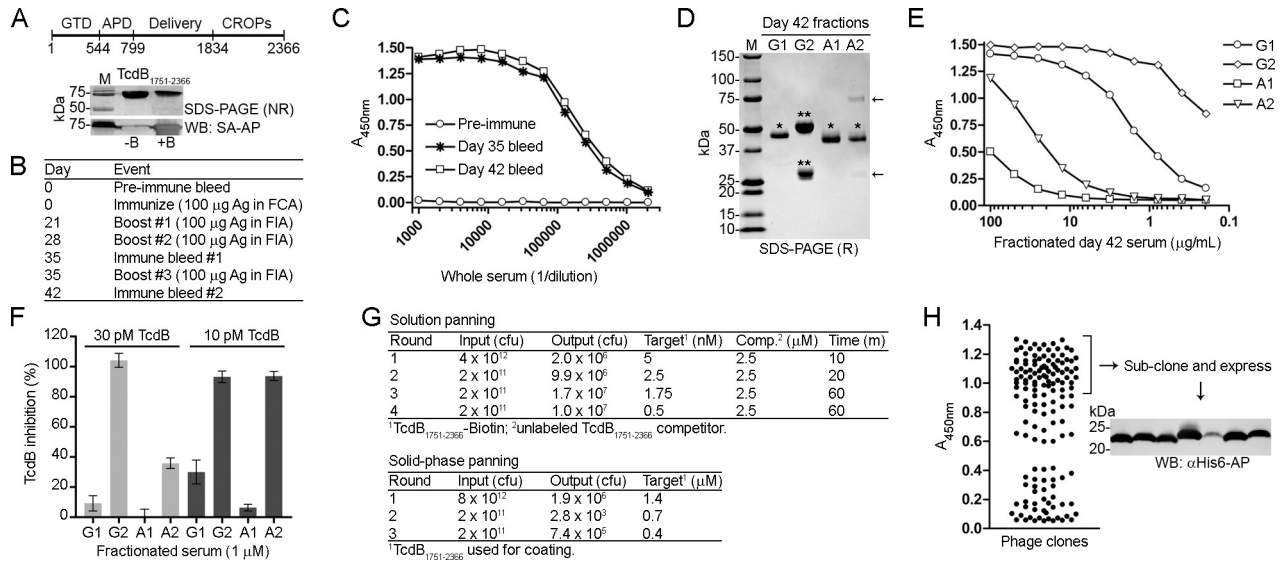


**Fig 1. Isolation of high-affinity TcdB-binding V<sub>H</sub>Hs.** (A, top) Schematic of TcdB. GTD, glucosyltransferase domain; APD, autoprotease domain, Delivery, delivery/receptor binding domain, CROPs, combined repetitive oligopeptides domain. (A, bottom) A 71.6 kDa fragment of *C. difficile* toxin B (TcdB<sub>1751-2366</sub>) was purified, biotinylated and analyzed by non-reducing (NR) SDS-PAGE and Western blot (WB) probed with streptavidin-AP (SA-AP). Approximately 1 μg of protein was loaded per lane. M, protein molecular weight marker; -B, unlabeled TcdB<sub>1751-2366</sub>; +B, biotinylated TcdB<sub>1751-2366</sub>. (B) TcdB<sub>1751-2366</sub> was used as an antigen (Ag) for llama immunization with the schedule shown. FCA, Freund's complete adjuvant; FIA, Freund's incomplete adjuvant. (C) ELISA showing the binding response from pre-immune and immune llama sera collected on days 35 and 42 post immunization to coated TcdB<sub>1751-2366</sub>. (D) Serum from day 42 post immunization was fractionated using protein G and protein A affinity columns and analyzed by SDS-PAGE under reducing (R) conditions. G1, A1 and A2 fractions contain heavy-chain IgG (hIgG, \*) while the G2 fraction contains conventional IgG (cIgG, \*\*). The arrows denote IgM heavy and light chains in the A2 fraction. (E) ELISA showing the binding response of fractionated day 42 serum to coated TcdB<sub>1751-2366</sub>. (F) Vero cell cytotoxicity assay demonstrating the effect of fractionated day 42 serum on TcdB inhibition, 72 h post addition of TcdB and polyclonal antibodies to Vero cell monolayers. TcdB was used at 10 and 30 pM and polyclonal fractionated sera at 1 μM. (G, top) Summary of solution-phase library panning titers using off-rate selection. In each round, the amount of target (biotinylated TcdB<sub>1751-2366</sub>) was reduced, the amount of competitor ("Comp"; unlabeled TcdB<sub>1751-2366</sub>) was held constant, and the incubation time of phage + target + competitor was increased. After incubation, the complex of phage and biotinylated TcdB<sub>1751-2366</sub> was captured on streptavidin coated microtiter plates, washed and eluted. (G, bottom) Summary of solid-phase library panning titers using coated TcdB<sub>1751-2366</sub>. (H) Phage ELISA showing binding of phage displayed V<sub>H</sub>Hs to coated TcdB<sub>1751-2366</sub>. V<sub>H</sub>Hs on phage producing the highest ELISA signals were expressed, purified and characterized. The Western blot (WB) shows detection of purified V<sub>H</sub>Hs with an α-His6-AP secondary antibody.

<https://doi.org/10.1371/journal.pone.0208978.g001>

selection, TcdB<sub>1751-2366</sub> was coated directly on standard microtiter plate wells, incubated with library phage and eluted with high pH. In each round of panning the amount of TcdB<sub>1751-2366</sub> coated was reduced. Monoclonal phage ELISA was performed on clones derived from both methods after three or four rounds of panning and those producing the highest ELISA signals were sequenced and sub-cloned for expression in *E. coli* (Fig 1H). A total of 29 unique V<sub>H</sub>H sequences (all differing in CDR3; S1 Table) were expressed and purified by immobilized metal-ion affinity chromatography (IMAC) with purification yields ranging from 3.1–41.3 mg/L before extensive biophysical characterization.

### Biophysical characterization of V<sub>H</sub>Hs

Size-exclusion chromatography (SEC) profiles of the V<sub>H</sub>Hs showed predominantly single monodispersed peaks devoid of higher order aggregates as expected (Table 1, Fig 2A and S1 Fig). Circular dichroism spectroscopy was used to determine V<sub>H</sub>H melting temperatures (*T<sub>m</sub>*s) and to assess V<sub>H</sub>H refolding (Table 1, Fig 2B and S2 Fig). The *T<sub>m</sub>*s ranged from 57.6 to 87.2 °C (median *T<sub>m</sub>* = 73.4 °C) and most V<sub>H</sub>Hs could refold, although the completeness of refolding was sequence dependent. V<sub>H</sub>H binding affinities and kinetics were determined by SPR single-cycle kinetic analysis (Table 1, Fig 2C and S3 Fig). V<sub>H</sub>H affinities (*K<sub>D</sub>*s) ranged

**Table 1. Biophysical properties of anti-TcdB V<sub>H</sub>Hs.**

V <sub>H</sub> H	Panning source	V <sub>c</sub> (mL)	SEC (%) <sup>a</sup>	T <sub>m</sub> (°C) <sup>b</sup>	k <sub>a</sub> (M <sup>-1</sup> s <sup>-1</sup> )	k <sub>d</sub> (s <sup>-1</sup> )	K <sub>D</sub> (nM)	R <sub>max</sub> (RU) <sup>c</sup>	Epitope bin
B26	solution	12.97	99.8	68.3±0.3	5.25×10 <sup>6</sup>	3.45×10 <sup>-2</sup>	6.3	149	4
B35	solution	14.07	99.8	76.2±0.4	1.16×10 <sup>6</sup>	1.05×10 <sup>-3</sup>	0.9	50	1
B39	solution	16.05	99.8	87.2±0.2	3.44×10 <sup>7</sup>	2.56×10 <sup>-3</sup>	0.07	43	1
B45	solution	14.84	99.4	79.5±0.4	3.52×10 <sup>6</sup>	3.84×10 <sup>-4</sup>	0.1	55	1
B46	solid phase	13.18	99.3	61.0±1.4	1.53×10 <sup>5</sup>	9.43×10 <sup>-3</sup>	62	51	n.d.
B48	both	13.07	99.7	82.5±0.3	4.11×10 <sup>6</sup>	5.71×10 <sup>-3</sup>	1.4	73	3
B52	both	12.77	99.9	65.3±0.7	1.29×10 <sup>7</sup>	1.01×10 <sup>-2</sup>	0.8	63	3
B53	solid phase	12.97	99.6	77.1±0.0	4.38×10 <sup>6</sup>	7.98×10 <sup>-3</sup>	1.8	72	3
B54	solution	12.85	95.3	81.7±0.3	3.86×10 <sup>7</sup>	1.47×10 <sup>-2</sup>	0.4	65	2
B55	solid phase	13.35	99.8	66.6±1.1	3.34×10 <sup>5</sup>	4.93×10 <sup>-2</sup>	147	142	n.d.
B56	solid phase	14.00	86.7	57.6±0.3	5.46×10 <sup>4</sup>	3.15×10 <sup>-2</sup>	576	18	n.d.
B65	solid phase	13.26	96.3	84.4±0.2	1.32×10 <sup>4</sup>	2.33×10 <sup>-3</sup>	176	17	n.d.
B69	solid phase	13.11	82.1	80.9±0.5	1.17×10 <sup>7</sup>	1.50×10 <sup>-1</sup>	12.8	102	5
B71	solid phase	12.88	85.9	63.3±0.3	7.76×10 <sup>6</sup>	9.18×10 <sup>-2</sup>	11.8	61	6
B73	both	13.41	99.7	80.2±0.0	1.27×10 <sup>7</sup>	9.19×10 <sup>-3</sup>	0.7	63	3
B74	both	13.62	99.6	75.0±0.2	1.23×10 <sup>7</sup>	3.58×10 <sup>-3</sup>	0.3	66	3
B76	solid phase	12.48	99.4	84.2±1.1	1.38×10 <sup>6</sup>	2.17×10 <sup>-1</sup>	157	74	n.d.
B79	solid phase	13.48	99.1	66.9±0.1	5.59×10 <sup>6</sup>	9.72×10 <sup>-3</sup>	1.7	75	3
B85	solution	12.94	99.4	69.7±0.1	1.93×10 <sup>7</sup>	1.14×10 <sup>-2</sup>	0.6	73	2
B86	solution	13.03	99.6	72.9±0.1	8.25×10 <sup>6</sup>	3.98×10 <sup>-3</sup>	0.5	71	3
B92	solid phase	12.85	98.9	78.0±0.1	1.51×10 <sup>6</sup>	8.28×10 <sup>-1</sup>	548	72	n.d.
B94	solution	12.58	96.7	69.7±0.4	6.19×10 <sup>5</sup>	8.77×10 <sup>-3</sup>	14.2	385	4
B95	solid phase	13.97	95.1	80.8±0.6	1.12×10 <sup>7</sup>	7.05×10 <sup>-3</sup>	0.6	72	3
B96	solution	13.17	99.7	70.5±0.2	1.37×10 <sup>6</sup>	7.33×10 <sup>-2</sup>	53.6	104	n.d.
B99	solution	13.05	98.7	69.8±2.2	6.33×10 <sup>7</sup>	1.04×10 <sup>-1</sup>	1.6	76	2
B131	solution	13.01	100	69.3±2.3	5.47×10 <sup>7</sup>	1.40×10 <sup>-1</sup>	2.6	73	7
B149	solution	13.45	97.4	83.9±0.0	4.12×10 <sup>4</sup>	2.20×10 <sup>-2</sup>	534	133	n.d.
B158	solution	13.44	99.4	73.4±0.8	3.44×10 <sup>4</sup>	1.74×10 <sup>-3</sup>	50.5	67	3
B167	solution	13.14	99.6	72.1±0.4	1.53×10 <sup>7</sup>	1.10×10 <sup>-3</sup>	0.07	76	2

<sup>a</sup>% monomer determined by area under the curve

<sup>b</sup>(mean ± SD)

<sup>c</sup>Observed R<sub>max</sub> was obtained from a TcdB surface with a theoretical R<sub>max</sub> of 200 RUs; n.d., not determined.

<https://doi.org/10.1371/journal.pone.0208978.t001>

from 70 pM to 576 nM and, when classified by selection method (Fig 2D), the 18 V<sub>H</sub>Hs isolated from solution panning were of statistically higher affinity than the 15 V<sub>H</sub>Hs obtained by solid-phase panning (median K<sub>D</sub>s of 0.79 nM and 12.3 nM, respectively, and note that the four V<sub>H</sub>Hs found by both selection methods were counted in each). Next, V<sub>H</sub>Hs with K<sub>D</sub>s of ~50 nM and stronger were subjected to epitope binning by SPR-based co-injection (V<sub>H</sub>H 1 followed by V<sub>H</sub>H 1 + V<sub>H</sub>H 2) experiments (Table 1, Fig 2E and S4 Fig). From the 21 V<sub>H</sub>Hs binned a total of seven non-overlapping TcdB epitopes were found (Fig 2F). The nine V<sub>H</sub>Hs residing in epitope bin E3 were clonally related (Fig 2F, S1 Table) while the other six bins contained predominantly unique, unrelated V<sub>H</sub>Hs. Finally, using V<sub>H</sub>Hs with the highest affinities and/or slowest off-rates (k<sub>d</sub>s) in each epitope bin (B39, B69, B71, B74, B94, B131 and B167), we examined the TcdB neutralization capacity in Vero cell assays. At the highest V<sub>H</sub>H concentration tested (1 μM) none of the antibodies were capable of inhibiting the cytotoxic effects of TcdB on cells at 1 pM.

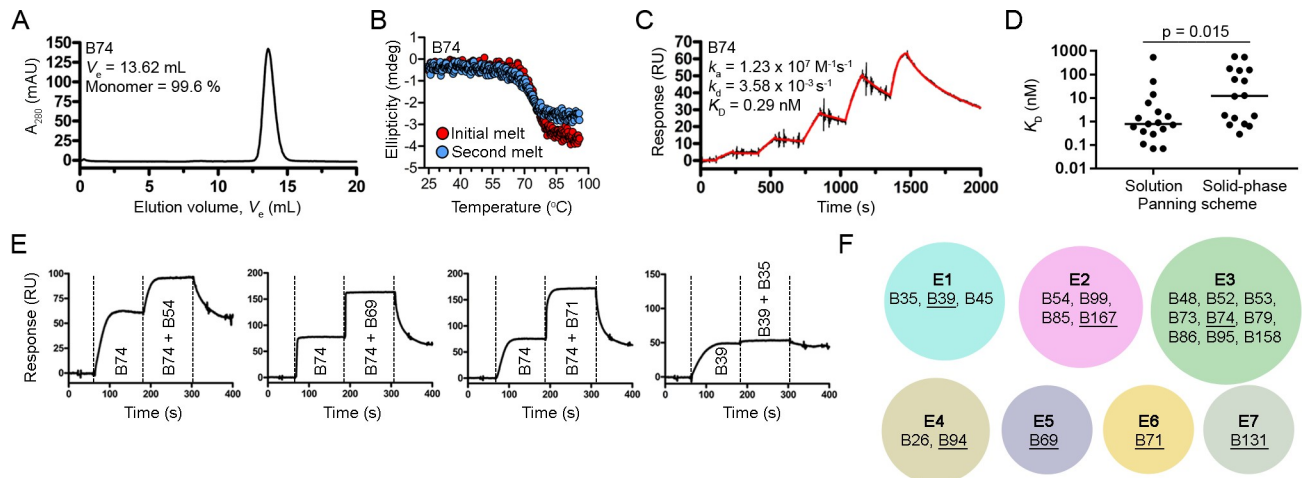


**Fig 2. Biophysical characterization of V<sub>H</sub>Hs.** Representative SEC profile (A) and thermal unfolding curve from initial and refolded thermal melts (B). (C) Representative SPR single-cycle kinetics sensorgram showed high-affinity binding of V<sub>H</sub>Hs to biotinylated TcdB<sub>1751-2366</sub> immobilized on a CAP sensor chip. (D) Plot comparing K<sub>D</sub>s of V<sub>H</sub>Hs isolated from solution and solid-phase panning schemes. The four V<sub>H</sub>Hs isolated from both panning schemes were included in the analyses. Bars represent the median K<sub>D</sub> and a P-value < 0.05 was considered significant (Mann Whitney two-tailed unpaired *t*-test). (E) Representative sensorgrams demonstrating SPR-based epitope binning. All V<sub>H</sub>Hs were injected at 10x K<sub>D</sub> concentrations. (F) Summary of the TcdB<sub>1751-2366</sub> epitope bins identified in this study by the pool of V<sub>H</sub>Hs tested. The V<sub>H</sub>Hs in each epitope (E) bin are noted and the underlined V<sub>H</sub>Hs represent the highest affinity and/or slowest dissociating antibodies in each bin.

<https://doi.org/10.1371/journal.pone.0208978.g002>

### Reformatting V<sub>H</sub>Hs as dimeric molecules

We next generated V<sub>H</sub>H-V<sub>H</sub>H dimers using the three highest affinity V<sub>H</sub>Hs that targeted unique epitopes (B39, B74 and B167) to determine if biparatopic designs could impart a measurable level of TcdB neutralization not seen with V<sub>H</sub>H monomers. All possible combinations of the three antibodies were created including homodimers (Fig 3A), with a standard 25 amino acid linker separating each V<sub>H</sub>H. Dimers were expressed in *E. coli*, purified by IMAC with yields ranging from 2.0 to 12.0 mg/L (Fig 3B) and assessed by SEC (Fig 3C) which revealed a predominantly single monodispersed species with the exception of B39/B74 and B39/B39 dimers that showed higher order aggregates. V<sub>H</sub>H-V<sub>H</sub>H dimer T<sub>m</sub>s ranged from 64.4 to 73.1 °C. SPR off-rate analysis demonstrated nearly irreversible bivalent binding to TcdB<sub>1751-2366</sub> surfaces for many of the dimers, approaching the instrument limit of detection (Table 2, Fig 3D). Vero cell neutralization assays using the dimers showed minor TcdB inhibition with all nine formats tested ranging from 3.2% (B39/B39) to 7.5% (B167/B39) maximum inhibition (Table 2, Fig 3E). The negative control T5/TC9 dimer did not inhibit TcdB and the benchmark control mAb MDX-1388 reached a maximum inhibition of 76.6%.

### Reformatting V<sub>H</sub>Hs as Fc fusions

Given the modest level of TcdB inhibition seen with the V<sub>H</sub>H-V<sub>H</sub>H dimers, we next explored if construction of larger molecules may lead to greater TcdB neutralizing potency. V<sub>H</sub>H-Fc fusions (Fig 4A) were constructed using each of the seven high-affinity V<sub>H</sub>Hs from distinct epitope bins (B39, B69, B71, B74, B94, B131 and B167). The designs consisted of a set of V<sub>H</sub>H-Fcs with a 15-residue human IgG1 hinge (EPKSCDKTHTCPPCP) and another set of complementary molecules with a 35 residue camel/llama γ2a hinge (EPKIPQPQPKPQPQ PQPQPKPQPKPEPECTCPKCP), to explore the possible advantages a longer, more flexible hinge may have on TcdB inhibition. The V<sub>H</sub>H-Fcs, denoted “V<sub>H</sub>H-hFc” for molecules containing the human hinge and “V<sub>H</sub>H-cFc” for molecules containing the camel hinge, were

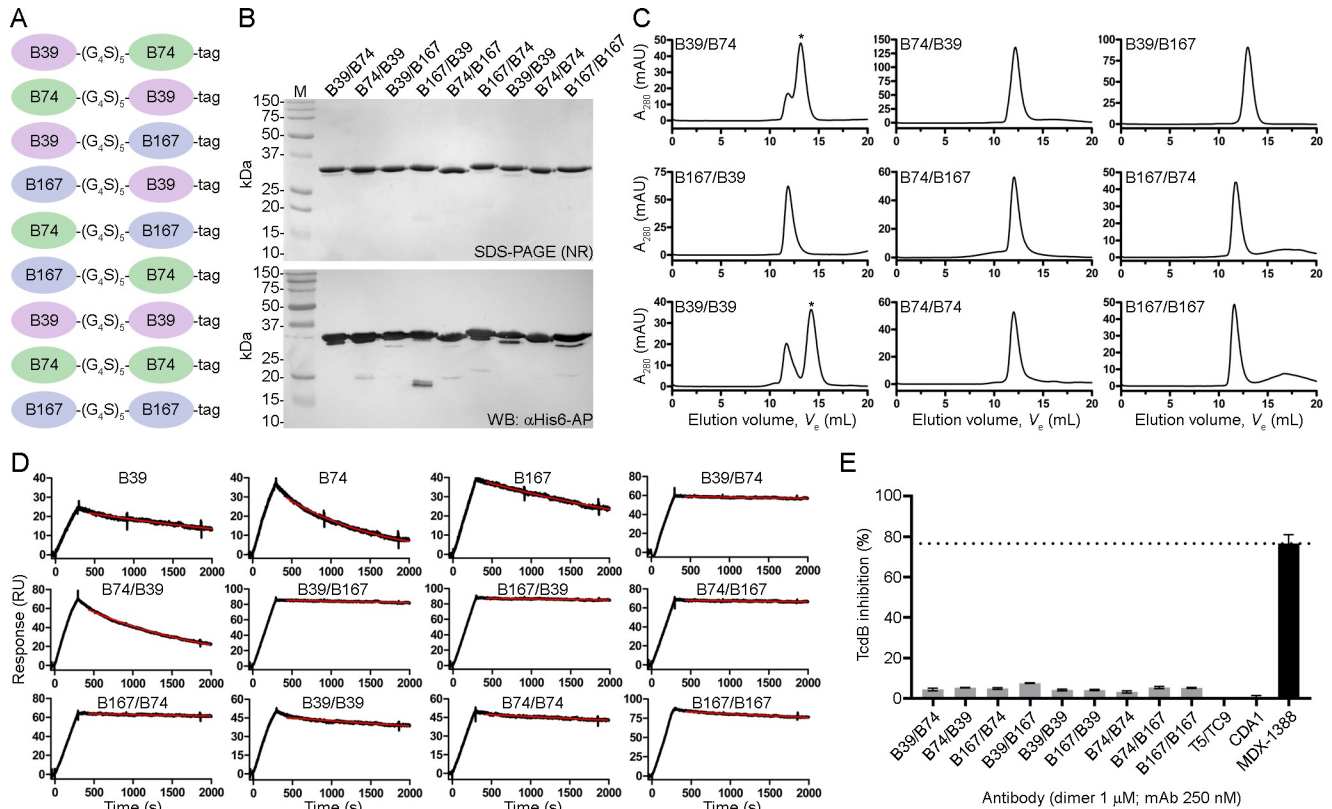


**Fig 3. Generation and characterization of V<sub>H</sub>H-V<sub>H</sub>H dimers.** (A) Cartoon diagram of V<sub>H</sub>H-V<sub>H</sub>H dimers separated by a 25 amino acid linker (G<sub>4</sub>S)<sub>5</sub> and containing a C-terminal His<sub>6</sub> “tag”. (B) Dimers were expressed, purified and analyzed by non-reducing (NR) SDS-PAGE and probed by α-His<sub>6</sub>-AP in Western blot (WB). M, protein molecular mass marker. (C) SEC profiles of dimers. Asterisks denote the peaks that were selected for SPR analysis when aggregates were present. (D) SPR sensorgrams showing dissociation phases of V<sub>H</sub>H-V<sub>H</sub>Hs and parent monomers. (E) TcdB neutralization with V<sub>H</sub>H-V<sub>H</sub>H dimers. The final TcdB concentration of 3–10 pM and V<sub>H</sub>H-V<sub>H</sub>H concentration of 1 μM was co-incubated with Vero cell monolayers for 72 h before addition of WST-1 cytotoxicity reagent. MDX-1388 was used at 250 nM. Neutralization values are presented as mean ± SD from n = 3 independent experiments.

<https://doi.org/10.1371/journal.pone.0208978.g003>

expressed in mammalian cells and purified by protein A with yields ranging from 2.5 to 21.6 mg/100 mL of culture (Table 3, Fig 4B). SEC analyses of V<sub>H</sub>H-Fcs revealed single, monodispersed peaks and consistently showed V<sub>H</sub>Hs with camel hinges eluting earlier, most likely due to their larger hydrodynamic radius (Table 3, Fig 4C and S5A Fig). SPR-determined off-rates demonstrated nearly irreversible bivalent binding to TcdB<sub>1751-2366</sub> surfaces (Table 3, Fig 4D and S5B Fig). Comparison of the off-rates (k<sub>off</sub>) of V<sub>H</sub>H-Fcs with human or camel hinges did not reveal significant differences in their ability to bind TcdB<sub>1751-2366</sub> (Fig 4E).

### TcdB neutralization with V<sub>H</sub>H-Fcs

The neutralization potencies of V<sub>H</sub>H-Fcs were compared to the benchmark mAb bezlotoxumab (MDX-1388) in TcdB inhibition assays using 500 fM TcdB and 250 nM antibody (Table 3, Fig 5A and 5B). MDX-1388 showed a maximum TcdB inhibition of 70.7% compared to V<sub>H</sub>H-Fcs that ranged from 8.9% (B71-cFc) to 61.2% (B94-cFc). There were essentially no differences between the neutralizing capacities of V<sub>H</sub>H-Fcs containing the short IgG1 hinge or the longer camel hinge, mirroring the near identical off-rates determined by SPR. Neither format of B39-Fc neutralized TcdB. CDA1 (an anti-TcdA mAb) [36] was included as a negative control and did not neutralize TcdB as expected. To examine possible synergistic

**Table 2. Biophysical properties of anti-TcdB V<sub>H</sub>H-V<sub>H</sub>H dimers.**

V <sub>H</sub> H- V <sub>H</sub> H	Yield (mg/L) <sup>a</sup>	V <sub>e</sub> (mL) <sup>b</sup>	T <sub>m</sub> (°C) <sup>c</sup>	k <sub>d</sub> (s <sup>-1</sup> )	Maximum TcdB neutralization (%) <sup>c,d</sup>
B39/B74	9.2	13.2	71.6 ± 0.2	2.2 × 10 <sup>-5</sup>	4.4 ± 0.4
B74/B39	3.6	12.2	70.9 ± 1.6	5.9 × 10 <sup>-4</sup>	5.3 ± 0.1
B39/B167	9.0	13.0	73.1 ± 1.7	2.4 × 10 <sup>-5</sup>	4.9 ± 0.3
B167/B39	2.0	11.9	67.7 ± 1.4	1.7 × 10 <sup>-5</sup>	7.5 ± 0.1
B74/B167	5.8	12.0	64.4 ± 2.1	1.4 × 10 <sup>-5</sup>	4.2 ± 0.2
B167/B74	2.4	11.7	66.5 ± 0.6	2.4 × 10 <sup>-5</sup>	4.1 ± 0.2
B39/B39	12.0	14.2	79.5 ± 3.4	9.7 × 10 <sup>-5</sup>	3.2 ± 0.3
B74/B74	2.2	12.0	70.4 ± 3.3	6.3 × 10 <sup>-5</sup>	5.4 ± 0.3
B167/B167	6.8	11.6	67.5 ± 2.3	6.0 × 10 <sup>-5</sup>	5.1 ± 0.2
MDX-1388	-	n.d.	n.d.	n.d.	76.6 ± 4.4 <sup>c</sup>

<sup>a</sup>Purification yield from 1 L *E. coli* culture

<sup>b</sup>V<sub>e</sub> from Superdex 200

<sup>c</sup>(mean ± SD)

<sup>d</sup>1 μM or

<sup>e</sup>250 nM antibody + 3 pM TcdB vero cell cytotoxicity (72 h); n.d., not determined.

<https://doi.org/10.1371/journal.pone.0208978.t002>

effects from combinations of V<sub>H</sub>H-Fcs on TcdB inhibition, pairs of V<sub>H</sub>H-Fcs (125 nM + 125 nM) were examined in neutralization assays (S2 Table, Fig 5A and 5B). The V<sub>H</sub>H-Fc pair of B94-hFc + B167-hFc achieved a maximum TcdB inhibition of 76.2%, slightly exceeding the neutralization potency of each V<sub>H</sub>H-Fc alone and that of MDX-1388. In pairs containing B39-Fc, the non-neutralizing antibody, overall neutralization was reduced by approximately 50% of the maximum inhibiting potency of the second antibody partner, reflecting the fact that 50% less inhibitory antibody was present (Fig 5A and 5B).

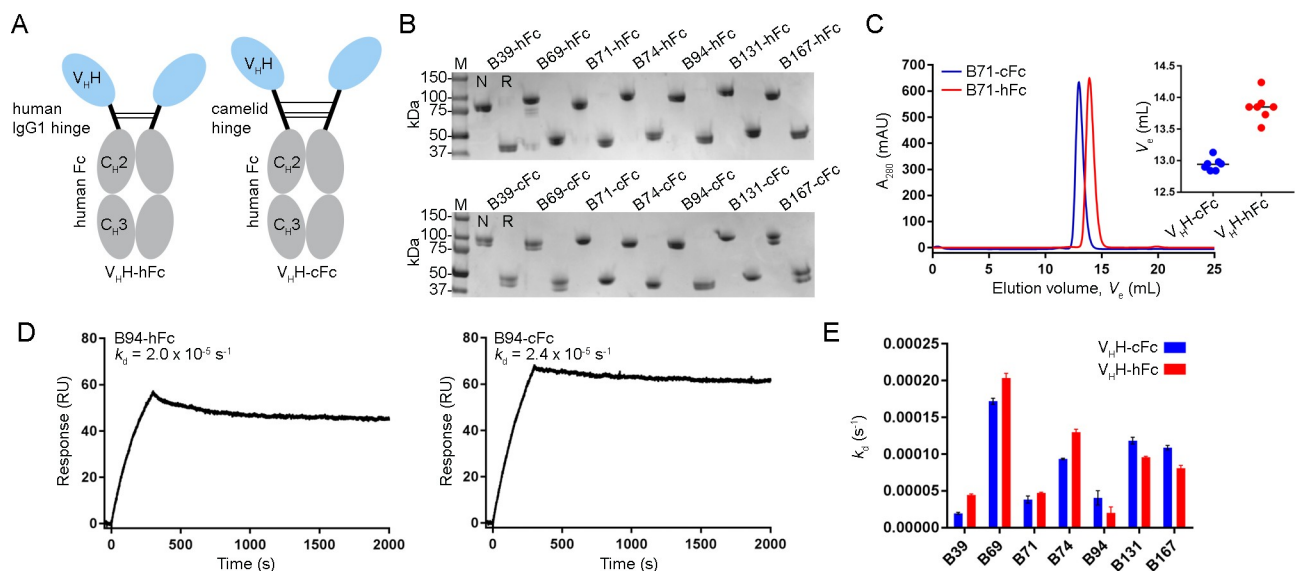


**Fig 4. Generation and characterization of V<sub>H</sub>H-Fcs with human or camelid hinges.** (A) Cartoon diagram illustrating the two V<sub>H</sub>H-Fc formats used with varying hinge length and composition. (B) Purified V<sub>H</sub>H-Fcs were analyzed by SDS-PAGE under non-reducing (N) and reducing (R) conditions. (C) Representative V<sub>H</sub>H-Fc SEC elution profile from a Superdex 200 column. *Inset*, plot of SEC elution volumes for all V<sub>H</sub>H-cFc and V<sub>H</sub>H-hFc. (D) Representative SPR sensorgrams showing 30 min (1800 s) dissociations of V<sub>H</sub>H-Fc fusions flowing over immobilized TcdB<sub>1751-2366</sub> surfaces. (E) Dissociation rate comparison of V<sub>H</sub>H-Fcs with human or camelid hinges.

<https://doi.org/10.1371/journal.pone.0208978.g004>

**Table 3. Biophysical properties of anti-TcdB V<sub>H</sub>H-Fc fusions.**

V <sub>H</sub> H-Fc/mAb	Hinge	Yield (mg/ 100 mL) <sup>a</sup>	V <sub>e</sub> (mL) <sup>b</sup>	k <sub>d</sub> (s <sup>-1</sup> )	Maximum TcdB neutralization (%) <sup>c,d</sup>
B39-hFc	human	5.7	17.64	4.5 × 10 <sup>-5</sup>	0.0
B69-hFc	human	13	14.24	2.0 × 10 <sup>-4</sup>	18.0 ± 10.2
B71-hFc	human	6	13.91	4.7 × 10 <sup>-5</sup>	11.0 ± 7.0
B74-hFc	human	4.4	13.82	1.3 × 10 <sup>-4</sup>	26.3 ± 4.5
B94-hFc	human	12.2	13.52	2.0 × 10 <sup>-5</sup>	55.9 ± 22.4
B131-hFc	human	14.6	13.70	9.6 × 10 <sup>-5</sup>	18.0 ± 13.4
B167-hFc	human	2.5	13.85	8.1 × 10 <sup>-5</sup>	37.5 ± 2.7
B39-cFc	camelid	7.9	15.07	2.0 × 10 <sup>-5</sup>	0.1 ± 0.1
B69-cFc	camelid	9.1	13.13	2.0 × 10 <sup>-4</sup>	20.2 ± 5.7
B71-cFc	camelid	11.3	12.98	4.7 × 10 <sup>-5</sup>	8.9 ± 5.5
B74-cFc	camelid	6.8	12.95	9.4 × 10 <sup>-5</sup>	22.3 ± 4.2
B94-cFc	camelid	11.8	12.84	2.4 × 10 <sup>-5</sup>	61.2 ± 1.3
B131-cFc	camelid	21.6	12.84	9.6 × 10 <sup>-5</sup>	18.7 ± 12.3
B167-cFc	camelid	9.2	12.90	8.1 × 10 <sup>-5</sup>	22.8 ± 2.9
MDX-1388	human	-	n.d.	n.d.	70.7 ± 13.9

<sup>a</sup>Purification yield from 100 mL HEK293 culture

<sup>b</sup>V<sub>e</sub> from Superdex 200

<sup>c</sup>(mean ± SD)

<sup>d</sup>250 nM antibody + 500 fM TcdB vero cell cytotoxicity (72 h); n.d., not determined.

<https://doi.org/10.1371/journal.pone.0208978.t003>

### V<sub>H</sub>H-Fc competition with bezlotoxumab

To determine if our panel of neutralizing V<sub>H</sub>H-Fcs recognized similar or unique TcdB epitopes from that of bezlotoxumab we performed SPR co-injection experiments (Fig 5C and 5D). B39-hFc, B69-hFc, B71-hFc and B74-hFc did not compete with MDX-1388 in either injection sequence, indicating that the four V<sub>H</sub>H-Fcs bind sites on TcdB completely independent of the MDX-1388 binding site. This is unsurprising for B39-hFc given the inability of this antibody to neutralize TcdB. The other three V<sub>H</sub>Hs were previously shown to bind unique epitopes as monomers (Fig 2F) suggesting B69-hFc, B71-hFc and B74-hFc recognize three novel TcdB epitopes that support neutralizing antibodies. The results of B94-hFc, B131-hFc and B167-hFc binning with MDX-1388 revealed significant overlap in TcdB binding patterns. When MDX-1388 was injected first, B94-hFc was partially blocked by pre-bound MDX-1388 and B131-hFc and B167-hFc were completely blocked by pre-bound MDX-1388. In the opposite orientation, MDX-1388 binding was completely blocked by pre-bound B94-hFc, and partially blocked by pre-bound B131-hFc or B167-hFc. Collectively this data suggests the most potent TcdB neutralizing V<sub>H</sub>H-Fcs (B94-hFc, B167-cFc) bind TcdB at sites that partially overlap with the MDX-1388 binding site at the N-terminal end of the CROPs domain [27].

### Discussion

In this work we set out to identify high-affinity V<sub>H</sub>Hs capable of neutralizing *C. difficile* TcdB. We previously failed to identify monomeric V<sub>H</sub>H neutralizers when immunizing with a small C-terminal fragment of the CROPs domain [10]. Here our expanded immunogen design containing a portion of the central delivery domain and the entire CROPs domain yielded a number of V<sub>H</sub>Hs that were capable of TcdB inhibition when formatted as dimers and more so as Fc fusions. It should be noted that our previous TcdB-binding V<sub>H</sub>Hs [10] were not tested as V<sub>H</sub>H-Fc fusions and may have been capable of TcdB inhibition, although their affinities were

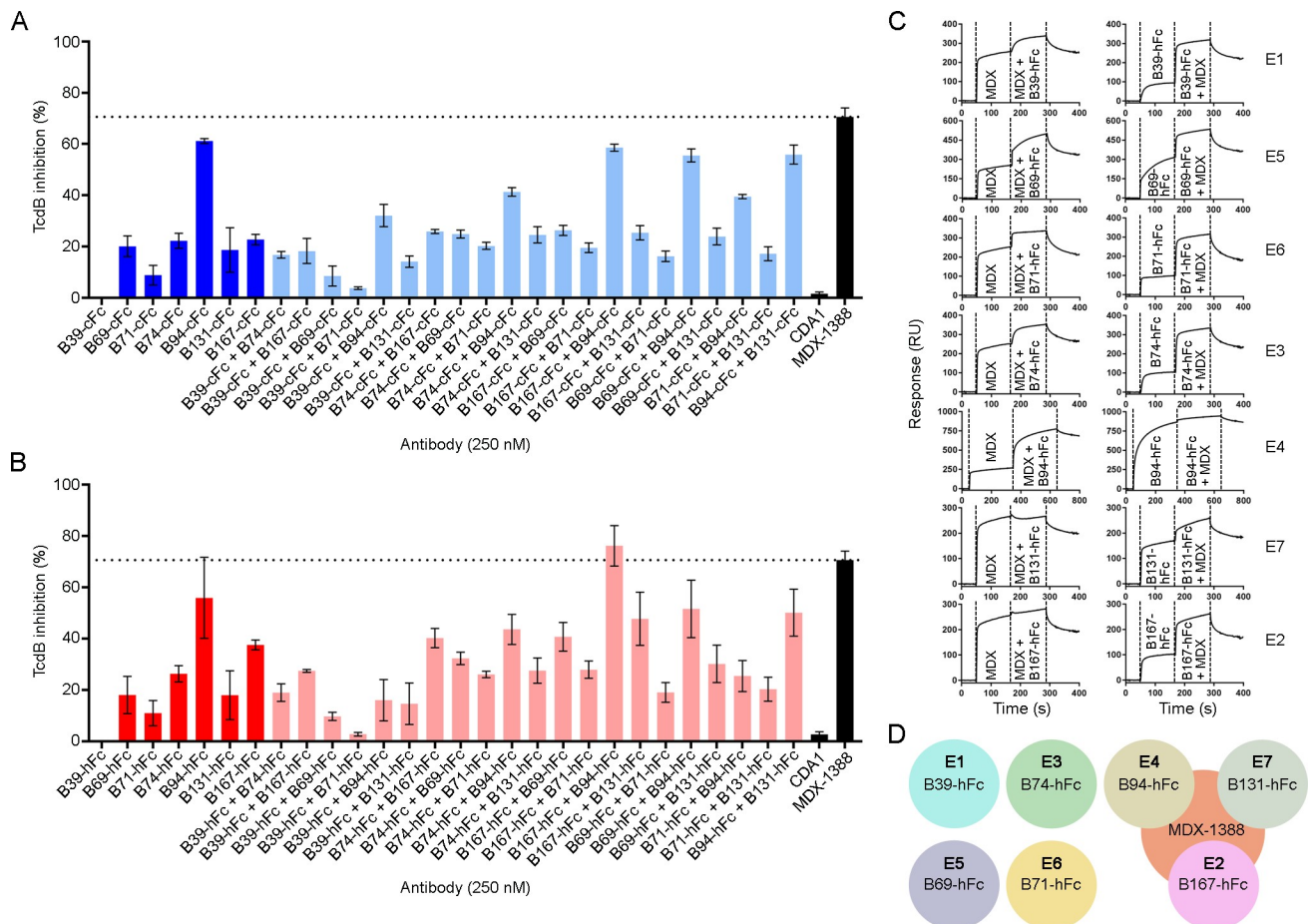


**Fig 5. TcdB neutralization assays with V<sub>H</sub>H-Fcs.** (A) TcdB neutralization with V<sub>H</sub>H-Fcs containing a camelid hinge. (B) TcdB neutralization with V<sub>H</sub>H-Fcs containing a human hinge. In (A) and (B), the final TcdB concentration of 500 fM and final antibody concentration of 250 nM (single antibody) or 125 + 125 nM (pairs) were co-incubated with Vero cell monolayers for 72 h before addition of WST-1 cytotoxicity reagent. Neutralization values are presented as mean ± SD from n = 4 independent experiments. (C) Sensorgrams showing SPR-based epitope binning of MDX-1388 mAb with each V<sub>H</sub>H-Fc, in both orientations, with antibodies injected at 25–50 × K<sub>D</sub> concentrations over TcdB<sub>1751-2366</sub> surfaces. Epitope bins corresponding to each V<sub>H</sub>H-Fc are noted. (D) Summary of V<sub>H</sub>H-Fc reactivity to TcdB<sub>1751-2366</sub> illustrating that several V<sub>H</sub>H-Fcs bind TcdB at sites distinct from MDX-1388, while others bind TcdB at regions that partially overlap with MDX-1388.

<https://doi.org/10.1371/journal.pone.0208978.g005>

considerably weaker than the V<sub>H</sub>Hs isolated in this work. Once again the monomeric V<sub>H</sub>Hs did not inhibit TcdB, suggesting a steric element that is required for TcdB inhibition when targeting the CROPs domain. Consistent with our findings, Yang *et al* isolated several TcdB-binding V<sub>H</sub>Hs and found five high-affinity V<sub>H</sub>Hs targeting the C-terminal CROPs domain that failed to inhibit TcdB cytotoxicity while those targeting the N-terminal GTD domain were potent neutralizers [13].

Our work is not the first to report TcdB-inhibiting V<sub>H</sub>Hs binding the CROPs domain. Andersen *et al* isolated several inhibitory monomeric V<sub>H</sub>Hs binding this domain, indicating that TcdB neutralization is possible with monomeric antibodies [15]. It is not clear how they successfully identified V<sub>H</sub>Hs that recognize critical epitope(s) for TcdB function/cell binding, that were not identified here, in our early work [10] or by [13], while employing a similar immunization strategy. Interestingly two of their non-neutralizing CROPs-binding V<sub>H</sub>Hs were converted into inhibitory antibodies when displayed on the surfaces of lactobacilli [15], again pointing to a large steric element in imparting TcdB inhibition with antibodies binding this region of the toxin.

Beyond V<sub>H</sub>Hs there are several potent TcdB-neutralizing mAbs that have been well studied. The most advanced anti-TcdB mAb is bezlotoxumab which received FDA approval for recurrent *C. difficile* infection in 2016. This antibody was originally isolated in a study reported by [36] and demonstrated to bind the C-terminal receptor binding domain (CROPs domain). Structural studies performed by [27] revealed the precise binding site of the mAb lies within the first two of four CROP repeat domains, with each CROP domain consisting of three short repeating units (SRs) followed by one long repeating unit (LR) and two more SRs. SPR binding data showed bezlotoxumab bound two distinct epitopes which was later supported by X-ray crystal structures and homology modeling showing two Fab fragments binding adjacent to each other in the N-terminal half of the CROPs domain (aa 1834–2101). Given bezlotoxumab neutralizes TcdB by preventing binding to mammalian cells [27,37], one can assume that some of our most potent V<sub>H</sub>H-Fc fusions (B94-Fc, B131-Fc and B167-Fc) neutralize TcdB in a similar manner given that they partially overlap with bezlotoxumab for TcdB binding. Whether the exact mechanism of inhibition is due to blocking putative carbohydrate binding site interactions with a host-cell receptor, or by steric effects precluding the central/delivery domain from making contacts with FZD2, PVRL3 or CSPG4 receptors is unknown. It is interesting to note that the observed  $R_{\max}$  of B94 in SPR experiments was considerably higher than other antibodies as both a V<sub>H</sub>H monomer (Table 1) and as a V<sub>H</sub>H-Fc in binning experiments (Fig 5C), suggesting that B94 may bind to repeating TcdB CROPs domain epitopes. Supporting this idea is the fact that B94-Fc was the only V<sub>H</sub>H-Fc to completely block MDX-1388 binding when B94-Fc was bound to TcdB first. If a repeating epitope is bound by B94-Fc, it would suggest a similar mechanism of inhibition to that of MDX-1388 and that affinity improvements may lead to greater neutralizing potency since the monovalent affinity of B94 is relatively weak ( $K_D = 14$  nM) compared to a Fab fragment from MDX-1388 ( $K_D = 19$  pM or 370 pM; depending on the TcdB epitope) [27].

For the other three neutralizing V<sub>H</sub>H-Fcs described here (B69-Fc, B71-Fc and B74-Fc) their location for toxin binding and subsequently their mechanism for toxin inhibition also remain unknown. B39, which failed to neutralize TcdB as an Fc fusion and did not overlap with bezlotoxumab as expected, was previously [12] co-crystallized with a C-terminal fragment of the TcdB CROPs domain (aa 2248–2367 of TcdB from strain 10463) and definitively showed only recognition of a single, non-repeating TcdB epitope. This may suggest that antibodies binding at a distance from the central delivery/translocation domain have minimal effects on TcdB inhibition compared to antibodies binding nearby in the N-terminal half of the CROPs domain. Elsewhere, [28] have successfully identified four inhibitory mAbs targeted to the CROPs domain of TcdB that were neutralizers alone and to a greater extent when combined in pairs. Additionally, TcdB-neutralizing mAbs recognizing the C-terminal GT domain of TcdB have proven to be both potent inhibitors and effective in *in vivo* protection assays [38,39,40].

There were several other interesting observations of note from this work. The conventional IgG (cIgG) fraction obtained from llama serum post immunization with TcdB<sub>1751-2366</sub> was capable of inhibiting TcdB in cytotoxicity assays more efficiently than the three heavy-chain IgG (hcIgG) fractions. While the cIgG binding titer for TcdB was higher than the best hcIgG fraction by approximately 10-fold, which is a typical binding pattern we have observed in several other immunization campaigns, there were dramatic differences in the inhibition pattern seen between G1 (hcIgG) and G2 (cIgG) fractions. It is possible that a greater agglutination mechanism with camelid cIgGs compared to camelid hcIgGs is at play here and could be due to the physical distance separating the binding arms of each antibody format. We hypothesize that the more compact hcIgG footprint may bias the polyclonal pool toward intra-toxin binding events and that the greater distance afforded to cIgGs promotes both intra-toxin and inter-

toxin binding events, leading to increased agglutination and ultimately greater TcdB inhibition. Supporting this is the fact the A2 (hIgG) fraction, which showed a much weaker TcdB binding titer than the G1 fraction, possessed considerably greater neutralizing potency likely driven by IgM antibodies found as contaminants in the fractionated serum.

We performed panning experiments in solution using off-rate based selection and this method produced statistically higher affinity V<sub>H</sub>Hs compared to panning on immobilized antigen. This method of selection was also the source of the V<sub>H</sub>H-Fcs with the highest neutralizing potency, even though two of the three most potent TcdB inhibitors did not possess the highest overall monovalent V<sub>H</sub>H affinities. It is probable that the solution panning scheme presented the randomly biotinylated TcdB in a more native-like conformation and made more areas of the protein available for V<sub>H</sub>H binding compared to selection of V<sub>H</sub>Hs on TcdB-coated wells. This may explain the higher average binding affinity and greater neutralization potency of V<sub>H</sub>Hs isolated by the solution panning approach. We also examined the use of a longer camel hinge in place of the human IgG1 hinge to present the V<sub>H</sub>H in a more natural context when tethered to the Fc domain. While SEC profiles clearly showed that V<sub>H</sub>H-Fcs with camel hinges eluted earlier and thereby suggest a larger hydrodynamic volume, similar dissociation rate constants and TcdB neutralizing potency demonstrated there was no clear benefit to using the longer hinge. We do not completely understand why this was the case but speculate that the camel hinge only moderately expands the binding distance between V<sub>H</sub>H arms, still less than the footprint of a cIgG, and that neutralization is dependent on combination of factors including the location, geometry and accessibility of TcdB epitopes.

In summary, the V<sub>H</sub>Hs described here were potent TcdB neutralizing antibodies on par with bezlotoxumab when formatted as Fc fusions. We envision creating even more effective TcdB-neutralizing agents through optimization of affinities and binding geometries, such as through structure-guided biparatopic designs. Combining anti-TcdB biparatopic V<sub>H</sub>H-V<sub>H</sub>H designs with TcdA-neutralizing V<sub>H</sub>Hs onto a human Fc scaffold would allow for the generation of ultra-potent toxin inhibitors in a single antibody format, similar to approaches described previously [13,17], while maintaining the steric requirements for TcdB neutralization and long serum half-life. The *in vivo* efficacy previously demonstrated with multivalent designs that include linking anti-TcdA and anti-TcdB V<sub>H</sub>Hs suggests the inclusion of GTD-targeting anti-TcdB antibodies is critical [13,17,18]. Our results make a case for targeting the central delivery and CROPs domains with V<sub>H</sub>Hs. Whether including CROPs-targeting V<sub>H</sub>Hs in these designs will be as potent as those targeting the GTD region remains to be seen. In addition, finer epitope mapping of the V<sub>H</sub>H-Fcs that bound TcdB at regions distinct from bezlotoxumab will reveal if these antibodies recognize the central delivery domain or the CROPs domain and the nature of these unique inhibitory epitopes. Finally, the V<sub>H</sub>Hs described here will serve as useful additions to the reagent toolkit for further refinement of the mechanism of TcdB-host cell interactions.

## Supporting information

**S1 Fig. SEC chromatograms of V<sub>H</sub>H monomers.** V<sub>H</sub>Hs were passed over a Superdex 75 column at a flow rate of 0.5 mL/min in HBS-EP buffer. Molecular mass standards are shown. The percent monomer was calculated from the peak area under the curve.  $V_e$ , elution volume. (TIF)

**S2 Fig. Thermal unfolding of V<sub>H</sub>H monomers by circular dichroism spectroscopy.** (A) Thermal unfolding of V<sub>H</sub>Hs (50 µg/mL, 3.2 µM) was performed in phosphate buffer and measured in a 5 mm cuvette at 215 nm. V<sub>H</sub>Hs were allowed to cool at 25 °C for 3 h before the second thermal unfolding (refolded melting curve) was performed. (B) Voltage comparing two V<sub>H</sub>Hs (B54 and B99) that aggregate as a consequence of unfolding versus one V<sub>H</sub>H that does

not (B53).  
(TIF)

**S3 Fig. Single-cycle kinetics sensorgrams showing monomeric V<sub>H</sub>Hs binding to TcdB<sub>1751-2366</sub> surfaces.** Black lines represent raw data and red lines represent 1:1 binding model fits. Rate constants and affinities are shown for each antibody. The irrelevant V<sub>H</sub>H served as a negative control. For experimental conditions see [Materials and methods](#).  
(TIF)

**S4 Fig. Representative sensorgrams from SPR-based epitope binning of V<sub>H</sub>H monomers on TcdB<sub>1751-2366</sub> surfaces.** The first V<sub>H</sub>H was injected at 10×  $K_D$  concentration followed immediately by injection of a mixture of the first V<sub>H</sub>H + second V<sub>H</sub>H at 10×  $K_D$  concentration. For experimental conditions see [Materials and methods](#).  
(TIF)

**S5 Fig. Characterization of V<sub>H</sub>H-Fc fusions.** (A) SEC chromatograms of V<sub>H</sub>H-Fcs on a Superdex 200 column at a flow rate of 0.5 mL/min in HBS-EP buffer. (B) SPR sensorgrams illustrating the dissociation of 1 nM V<sub>H</sub>H-Fcs from TcdB<sub>1751-2366</sub> surfaces. For experimental conditions see [Materials and methods](#).  
(TIF)

**S1 Table. Clonal relatedness of TcdB-specific V<sub>H</sub>Hs isolated in this study.**  
(PDF)

**S2 Table. Select pairs of V<sub>H</sub>H-Fcs with the highest TcdB neutralization.**  
(PDF)

## Acknowledgments

We thank Kenneth Ng (University of Calgary) for providing the recombinant TcdB fragment, Shreya Jain (NRC) for assisting in protein expression and Yves Durocher and Denis L'Abbé (NRC) for producing the CDA1 and MDX-1388 control mAbs.

## Author Contributions

**Conceptualization:** Greg Hussack, C. Roger MacKenzie, Jamshid Tanha.

**Data curation:** Greg Hussack, Shannon Ryan, Henk van Faassen, Martin Rossotti.

**Formal analysis:** Greg Hussack, Shannon Ryan, Henk van Faassen, Martin Rossotti, C. Roger MacKenzie, Jamshid Tanha.

**Methodology:** Martin Rossotti.

**Resources:** C. Roger MacKenzie, Jamshid Tanha.

**Supervision:** Greg Hussack, C. Roger MacKenzie, Jamshid Tanha.

**Writing – original draft:** Greg Hussack.

**Writing – review & editing:** Greg Hussack, Shannon Ryan, Henk van Faassen, Martin Rossotti, C. Roger MacKenzie, Jamshid Tanha.

## References

1. Dubberke ER, Olsen MA (2012) Burden of *Clostridium difficile* on the healthcare system. *Clin Infect Dis* 55 Suppl 2: S88–92.

2. Hussack G, Tanha J (2016) An update on antibody-based immunotherapies for *Clostridium difficile* infection. *Clin Exp Gastroenterol* 9: 209–224. <https://doi.org/10.2147/CEG.S84017> PMID: 27536153
3. Napolitano LM, Edmiston CE Jr. (2017) *Clostridium difficile* disease: Diagnosis, pathogenesis, and treatment update. *Surgery* 162: 325–348. <https://doi.org/10.1016/j.surg.2017.01.018> PMID: 28267992
4. Hopkins RJ, Wilson RB (2018) Treatment of recurrent *Clostridium difficile* colitis: a narrative review. *Gastroenterol Rep* 6: 21–28.
5. Aktories K, Schwan C, Jank T (2017) *Clostridium difficile* toxin biology. *Ann Rev Microbiol* 71: 281–307.
6. Chandrasekaran R, Lacy DB (2017) The role of toxins in *Clostridium difficile* infection. *FEMS Microbiol Rev* 41: 723–750. <https://doi.org/10.1093/femsre/fux048> PMID: 29048477
7. Hussack G, Tanha J (2010) Toxin-specific antibodies for the treatment of *Clostridium difficile*: current status and future perspectives. *Toxins* 2: 998–1018. <https://doi.org/10.3390/toxins2050998> PMID: 22069622
8. Mullard A (2016) FDA approves antitoxin antibody. *Nat Rev Drug Discov* 15: 811.
9. Navalkele BD, Chopra T (2018) Bezlotoxumab: an emerging monoclonal antibody therapy for prevention of recurrent *Clostridium difficile* infection. *Biologics* 12: 11–21. <https://doi.org/10.2147/BTT.S127099> PMID: 29403263
10. Hussack G, Arbabi-Ghahroudi M, van Faassen H, Songer JG, Ng KK, MacKenzie R, et al. (2011) Neutralization of *Clostridium difficile* toxin A with single-domain antibodies targeting the cell receptor binding domain. *J Biol Chem* 286: 8961–8976. <https://doi.org/10.1074/jbc.M110.198754> PMID: 21216961
11. Hussack G, Keklikian A, Alsughayyir J, Hanifi-Moghaddam P, Arbabi-Ghahroudi M, van Faassen H, et al. (2012) A V(L) single-domain antibody library shows a high-propensity to yield non-aggregating binders. *Protein Eng Des Sel* 25: 313–318. <https://doi.org/10.1093/protein/gzs014> PMID: 22490957
12. Murase T, Eugenio L, Schorr M, Hussack G, Tanha J, Kitova EN, et al. (2013) Structural basis for antibody Recognition in the receptor-binding domains of toxins A and B from *Clostridium difficile*. *J Biol Chem* 289: 2331–2343. <https://doi.org/10.1074/jbc.M113.505917> PMID: 24311789
13. Yang Z, Schmidt D, Liu W, Li S, Shi L, Sheng J, et al. (2014) A novel multivalent, single-domain antibody targeting TcdA and TcdB prevents fulminant *Clostridium difficile* infection in mice. *J Infect Dis* 210: 964–972. <https://doi.org/10.1093/infdis/jiu196> PMID: 24683195
14. Shkoporov AN, Khokhlova EV, Savochkin KA, Kafarskaia LI, Efimov BA (2015) Production of biologically active scFv and VHH antibody fragments in *Bifidobacterium longum*. *FEMS Microbiol Lett* 362: fnv083.
15. Andersen KK, Strokappe NM, Hultberg A, Truusalu K, Smidt I, Mikelsaar RH, et al. (2015) Neutralization of *Clostridium difficile* toxin B mediated by engineered lactobacilli producing single domain antibodies. *Infect Immun* 84: 395–406. <https://doi.org/10.1128/IAI.00870-15> PMID: 26573738
16. Unger M, Eichhoff AM, Schumacher L, Strycio M, Menzel S, Schwan C, et al. (2015) Selection of nanobodies that block the enzymatic and cytotoxic activities of the binary *Clostridium difficile* toxin CDT. *Sci Rep* 5: 7850. <https://doi.org/10.1038/srep07850> PMID: 25597743
17. Schmidt DJ, Beamer G, Tremblay JM, Steele JA, Kim HB, Wang Y, et al. (2016) A tetraspecific VHH-based neutralizing antibody modifies disease outcome in three animal models of *Clostridium difficile* infection. *Clin Vaccine Immunol* 23: 774–784. <https://doi.org/10.1128/CVI.00730-15> PMID: 27413067
18. Yang Z, Shi L, Yu H, Zhang Y, Chen K, Saint Fleur A, et al. (2016) Intravenous adenovirus expressing a multi-specific, single-domain antibody neutralizing TcdA and TcdB protects mice from *Clostridium difficile* infection. *Pathog Dis* 74: ftw078. <https://doi.org/10.1093/femspd/ftw078> PMID: 27502696
19. Sulea T, Hussack G, Ryan S, Tanha J, Purisima EO (2018) Application of assisted design of antibody and protein therapeutics (ADAPT) improves efficacy of a *Clostridium difficile* toxin A single-domain antibody. *Sci Rep* 8: 2260. <https://doi.org/10.1038/s41598-018-20599-4> PMID: 29396522
20. Conrath KE, Lauwereys M, Galleni M, Matagne A, Frère JM, Kinne J, et al. (2001) Beta-lactamase inhibitors derived from single-domain antibody fragments elicited in the camelidae. *Antimicrob Agents Chemother* 45: 2807–2812. <https://doi.org/10.1128/AAC.45.10.2807-2812.2001> PMID: 11557473
21. Muyldermans S (2013) Nanobodies: natural single-domain antibodies. *Ann Rev Biochem* 82: 775–797. <https://doi.org/10.1146/annurev-biochem-063011-092449> PMID: 23495938
22. Iezzi ME, Policastro L, Werbach S, Podhajcer O, Canziani GA (2018) Single-domain antibodies and the promise of modular targeting in cancer imaging and treatment. *Front Immunol* 9: 273. <https://doi.org/10.3389/fimmu.2018.00273> PMID: 29520274
23. Chen P, Tao L, Wang T, Zhang J, He A, Lam KH, et al. (2018) Structural basis for recognition of frizzled proteins by *Clostridium difficile* toxin B. *Science* 360: 664–669. <https://doi.org/10.1126/science.aar1999> PMID: 29748286

24. Tao L, Zhang J, Meraner P, Tovaglieri A, Wu X, Gerhard R, et al. (2016) Frizzled proteins are colonic epithelial receptors for *C. difficile* toxin B. *Nature* 538: 350–355. <https://doi.org/10.1038/nature19799> PMID: 27680706
25. LaFrance ME, Farrow MA, Chandrasekaran R, Sheng J, Rubin DH, Lacy DB (2015) Identification of an epithelial cell receptor responsible for *Clostridium difficile* TcdB-induced cytotoxicity. *Proc Natl Acad Sci U S A* 112: 7073–7078. <https://doi.org/10.1073/pnas.1500791112> PMID: 26038560
26. Yuan P, Zhang H, Cai C, Zhu S, Zhou Y, Yang X, et al. (2015) Chondroitin sulfate proteoglycan 4 functions as the cellular receptor for *Clostridium difficile* toxin B. *Cell Res* 25: 157–168. <https://doi.org/10.1038/cr.2014.169> PMID: 25547119
27. Orth P, Xiao L, Hernandez LD, Reichert P, Sheth PR, Beaumont M, et al. (2014) Mechanism of action and epitopes of *Clostridium difficile* toxin B-neutralizing antibody bezlotoxumab revealed by X-ray crystallography. *J Biol Chem* 289: 18008–18021. <https://doi.org/10.1074/jbc.M114.560748> PMID: 24821719
28. Davies NL, Compson JE, Mackenzie B, O'Dowd VL, Oxbrow AK, Heads JT, et al. (2013) A mixture of functionally oligoclonal humanized monoclonal antibodies that neutralize *Clostridium difficile* TcdA and TcdB with high levels of in vitro potency shows in vivo protection in a hamster infection model. *Clin Vaccine Immunol* 20: 377–390. <https://doi.org/10.1128/CVI.00625-12> PMID: 23324518
29. Henry KA, Tanha J, Hussack G (2015) Identification of cross-reactive single-domain antibodies against serum albumin using next-generation DNA sequencing. *Protein Eng Des Sel* 28: 379–383. <https://doi.org/10.1093/protein/gzv039> PMID: 26319004
30. Baral TN, MacKenzie R, Arbabi Ghahroudi M (2013) Single-domain antibodies and their utility. *Curr Protoc Immunol* 103: Unit 2 17.
31. Hussack G, Hiram T, Ding W, Mackenzie R, Tanha J (2011) Engineered single-domain antibodies with high protease resistance and thermal stability. *PLoS One* 6: e28218. <https://doi.org/10.1371/journal.pone.0028218> PMID: 22140551
32. Rossotti MA, Gonzalez-Techera A, Guarnaschelli J, Yim L, Camacho X, Fernández M, et al. (2015) Increasing the potency of neutralizing single-domain antibodies by functionalization with a CD11b/CD18 binding domain. *MAbs* 7: 820–828. <https://doi.org/10.1080/19420862.2015.1068491> PMID: 26192995
33. Durocher Y, Perret S, Kamen A (2002) High-level and high-throughput recombinant protein production by transient transfection of suspension-growing human 293-EBNA1 cells. *Nucleic Acids Res* 30: E9. PMID: 11788735
34. Henry KA, Kandalaf H, Lowden MJ, Rossotti MA, van Faassen H, Hussack G, et al. (2017) A disulfide-stabilized human VL single-domain antibody library is a source of soluble and highly thermostable binders. *Mol Immunol* 90: 190–196. <https://doi.org/10.1016/j.molimm.2017.07.006> PMID: 28820969
35. Conrath KE, Wernery U, Muyldermans S, Nguyen VK (2003) Emergence and evolution of functional heavy-chain antibodies in Camelidae. *Dev Comp Immunol* 27: 87–103. PMID: 12543123
36. Babcock GJ, Broering TJ, Hernandez HJ, Mandell RB, Donahue K, Boatright N, et al. (2006) Human monoclonal antibodies directed against toxins A and B prevent *Clostridium difficile*-induced mortality in hamsters. *Infect Immun* 74: 6339–6347. <https://doi.org/10.1128/IAI.00982-06> PMID: 16966409
37. Yang Z, Ramsey J, Hamza T, Zhang Y, Li S, Yfantis HG, et al. (2015) Mechanisms of protection against *Clostridium difficile* infection by the monoclonal antitoxin antibodies actoxumab and bezlotoxumab. *Infect Immun* 83: 822–831. <https://doi.org/10.1128/IAI.02897-14> PMID: 25486992
38. Marozsan AJ, Ma D, Nagashima KA, Kennedy BJ, Kang YK, Arrigale RR, et al. (2012) Protection against *Clostridium difficile* infection with broadly neutralizing antitoxin monoclonal antibodies. *J Infect Dis* 206: 706–713. <https://doi.org/10.1093/infdis/jis416> PMID: 22732923
39. Anosova NG, Cole LE, Li L, Zhang J, Brown AM, Mundle S, et al. (2015) A combination of three fully human toxin A- and toxin B-specific monoclonal antibodies protects against challenge with highly virulent epidemic strains of *Clostridium difficile* in the hamster model. *Clin Vaccine Immunol* 22: 711–725. <https://doi.org/10.1128/CVI.00763-14> PMID: 25924765
40. Kroh HK, Chandrasekaran R, Rosenthal K, Woods R, Jin X, Ohi MD, et al. (2017) Use of a neutralizing antibody helps identify structural features critical for binding of *Clostridium difficile* toxin TcdA to the host cell surface. *J Biol Chem* 292: 14401–14412. <https://doi.org/10.1074/jbc.M117.781112> PMID: 28705932